arXiv:1701.02154v1 [cond-mat.quant-gas] 9 Jan 2017

Spin-orbit coupled interferometry with ring–trapped Bose–Einstein condensates.

J. L. Helm,[1] T. P. Billam,[2] A. Rakonjac,[1] S. L. Cornish,[1] and S. A. Gardiner[1]

[1]*Joint Quantum Center (JQC) Durham-Newcastle, Department of Physics, Durham University, Durham DH1 3LE, United Kingdom*

[2]*Joint Quantum Center (JQC) Durham-Newcastle, Department of Mathematics and Statistics, Newcastle University, Newcastle upon Tyne, NE1 7RU, United Kingdom*

(Dated: January 10, 2017)

We propose a method of atom-interferometry using a spinor Bose–Einstein (BEC) and the well-established experimental technique of time-varying magnetic fields as a coherent beam-splitter. Our protocol creates long-lived superpositional counterflow states, which are of fundamental interest and can be made sensitive to both the Sagnac effect and magnetic fields on the sub micro-Gauss scale. We split a ring-trapped condensate, initially in the $m_f = 0$ hyperfine sub-level, into superpositions of both internal spin state and condensate superflow, which are spin-orbit coupled. After interrogation a relative phase accumulation can be inferred from a population transfer to the $m_f = \pm 1$ states. Our protocol maximises the classical Fisher information, and owing to the adiabatic splitting it may be a good candidate for developing quantum enhanced interferometry schemes. We present numerical and analytical treatments of our system.

The endeavour to optimally apply matter-wave interferometry has generated many proposals and prototypes of ultra-sensitive rotational [1–6], gravitational/inertial [7–14] and gravity wave [15–17] detection protocols. Optimal protocols should fully exploit the characteristics of BECs and should aim to be Heisenberg limited through entanglement or number-squeezing [18, 19], and have globally equivalent classical and quantum Fisher information (CFI, QFI) [20]. These requirements are satisfied by the scheme described in Ref. [3], where a common-path geometry is used, ensuring entanglement via the spatial overlap of the arms of the interferometer and maximising QFI through the schemes spatial symmetry. Optical trapping allows us to exploit internal atomic spin degrees of freedom, in particular by allowing simultaneous trapping of atoms in different magnetic sublevels [21, 22]. A useful method of controlling such spinor condensates is topological vortex imprinting [23–28], where the texture of externally applied time-varying magnetic fields (B-fields) is embedded in the condensate's spin and, therefore, its phase. The B-fields used in this imprinting process are common to the majority of cold atom experiments, and are therefore readily available.

In this Letter we propose a method of matter-wave interferometry which splits a repulsively interacting spinor condensate into a superposition of both spin- and superflow- states, which are spin-orbit coupled. This spin-orbit coupled interferometry (SOCI) procedure uses topological vortex imprinting as a beam-splitter in the momentum and spin bases, achieved through the use of the time varying B-field [Fig. 1]. The "arms" of the interferometer are not necessarily spatially separate, allowing for the creation of a common-path interferometer, which is insensitive to a variety of perturbing factors due to its intrinsic symmetry. A noteworthy application of the common-path method is zero-area Sagnac interferometry (ZASI) [29, 30], often discussed as an alternative to the Michelson geometry for optical gravity-wave detection [31–33]. We first present the coupled equations of motion describing the spinor condensate, modified to account for a rotating frame of reference. We then consider the effect of the B-field in isolation, and how this applies to splitting (and recombining) the wavefunction into a spin-orbit coupled superposition.

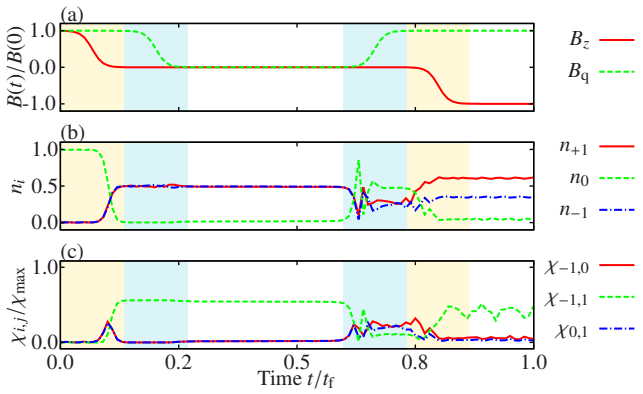

FIG. 1. (color online) Schematic of spin-orbit coupled interferometry (SOCI) procedure. (a) B-field ramping scheme. Yellow (outer) shaded regions highlight the beam-splitting processes during which the z bias field (B_z) is ramped down or up, while blue (inner) shaded regions show the phase unpinning processes during which the magnitude of the quadrupolar field (B_q) is ramped down or up. Numerically calculated norms, (b), and overlaps, (c), of the spinor components in the z-quantised basis for a $\delta = \pi$ interferometry run ending at time t_f.

This amounts to simply ramping down (and ramping up) the z bias field. We then show that an accumulated phase-difference between the counterflowing components translates to a population transfer from the field-insensitive eigenstate to the strong/weak-field-seeking eigenstates after a second beam-splitting procedure, and discuss how this population transfer can be measured.

A spin F condensate can most conveniently be treated as a system of $2F + 1$ coupled BECs. Here we will work only in the z-quantised (ZQ) representation, where all spin states are labelled with reference to the z-axis. For $F = -1/2$ our vector valued order parameter $\mathbf{\Psi}$ can be described in terms of the available spin-states, giving $\mathbf{\Psi} = \sum_{j=-1}^{1} \Psi_j |j\rangle$. The eigenvectors $|j\rangle$ satisfy $F_z|j\rangle = j|j\rangle$, and are simply the different possible values of the z-component of the spin. Here $\hbar F_z/2$ is the standard z direction angular momentum operator in the ZQ basis, resulting in spin-state eigenvectors $|1\rangle = (1, 0, 0)^T$, $|0\rangle =$

$(0,1,0)^T$, and $|-1\rangle = (0,0,1)^T$. In order to consider the effect of rotations, we introduce an angular momentum term describing the energy of a constant rotation characterised by the angular velocity vector $\mathbf{\Omega}$. As such, our full dynamical equations are

$$i\hbar\frac{\partial}{\partial t}\Psi_j = \left[-\frac{\hbar^2}{2m}\nabla^2 + V - i\hbar(\mathbf{r}\times\mathbf{\Omega})\cdot\nabla + g_{\rm n}\mathbf{\Psi}^\dagger\mathbf{\Psi}\right]\Psi_j + \left\{\left[g_{\rm s}\bar{\mathbf{F}}\cdot\mathbf{F} - \mu_{\rm B}g_F\mathbf{B}\cdot\mathbf{F}\right]\mathbf{\Psi}\right\}_j, \quad (1)$$

where the local spin vector $\bar{\mathbf{F}}$ has components $\bar{F}_\alpha = \Sigma_{j,k}\Psi_k^*\Psi_j\langle k|F_\alpha|j\rangle$. Here we have atomic mass m, Bohr magneton $\mu_{\rm B}$ and hyperfine gyromagnetic ratio g_F ($-1/2$ for ^{87}Rb in the $F=1$ manifold). The scattering terms are the normal interaction strength $g_{\rm n}$ and spin-spin interaction strength $g_{\rm s}$. The V term describes externally imposed optical trapping potentials. We consider a ring-trapped condensate with $V = m\omega_\perp^2[(\rho-R_0)^2+z^2]/2$, where $\rho = \sqrt{x^2+y^2}$, giving a radial trapping frequency $\omega_\perp$ and major radius R_0 (which will be described in terms of the harmonic oscillator length $a_\perp$). This potential simplifies our numerics, but the analysis only requires that the potential should be rotationally symmetric, with an optical plug covering $\rho = 0$ to prevent undesirable vortex dynamics. Gravity is taken to act in the z direction and could be included in the trapping potential without altering its symmetry, and so we do not consider it further. For our numerics we consider experimental parameters comparable to those described in Refs. [34, 35], however, for faster numerics we take the radial trapping frequency to be $\omega_\perp = 2\pi\times 80$ Hz, the major radius of the ring to be $R_0 = 5a_\perp = 6.02\,\mu$m, and the number of ^{87}Rb atoms to be $N = 10^4$. The normal binary scattering $g_{\rm n} = 4\pi\hbar^2(a_0+2a_2)/3m$ is a standard non-linear term based on the total local norm, where all spin-components may collide but their spins do not change or are merely exchanged, while $g_{\rm s} = 4\pi\hbar^2(a_2-a_0)/3m$ describes spin-flipping collisions which can result in population transfer, although the total spin must be conserved. Here a_0 and a_2 are the scattering lengths associated with binary elastic collisions in the total spin 0 and 2 channels respectively. Our numerics are for ^{87}Rb in the $F=1$ manifold, where $a_0 = 101.8a_{\rm B} \sim a_2 = 100.4a_{\rm B}$ [27], and $a_{\rm B}$ is the Bohr radius. For these interaction strengths, our system is ferromagnetic ($g_{\rm s}<0$), and its energy is minimised for maximal $|\bar{\mathbf{F}}|$. The splitting procedure generates a counterflow state for which $|\bar{\mathbf{F}}|=0$, and so minimises the Hamiltonian energy of anti-ferromagnetic ($g_{\rm s}>0$) systems [21]. As such, the counterflow state constitutes a metastable excited state for ferromagnetic systems, but would be a stable ground state for antiferromagnetic systems (e.g., ^{23}Na in $F=1$ or ^{87}Rb in $F=2$). However, since ^{87}Rb is only weakly ferromagnetic ($|g_{\rm s}|$ is comparatively small) the state's instability has a long associated timescale, and so the $g_{\rm s}$ term can be ignored in the analytics. We keep the $g_{\rm s}$ term in the numerics, observing only small deviations from the analytical result

The dominant dynamics of the system can be understood from the eigenvectors of the $\mathbf{B}\cdot\mathbf{F}$ operator, in turn determined by the texture of the magnetic field. Our fundamental requirement is that the B-field should have a non-trivial topology, such that a curve encircling the origin has non-zero winding number. This requirement is satisfied by either an anti-Helmholtz (aH) or Ioffe-Pritchard (IP) coil configuration. We consider the geometrically simpler IP configuration, which is quadrupolar in the x-y plane, but note that the same phenomena should be observable using the aH configuration. The IP B-field texture is best described in cylindrical spatial coordinates ρ,ϕ,z. The Cartesian components can then be written as $\mathbf{B}_{\rm IP} = (B_{\rm q}(\rho)\cos(\phi), -B_{\rm q}(\rho)\sin(\phi), B_z)$, where the quadrupolar field $B_{\rm q}(\rho) = b'\rho$ varies linearly with ρ and the z bias field is spatially uniform. Hence

$$\mathbf{B}\cdot\mathbf{F} = \begin{pmatrix} B_z & B_{\rm q}\,{\rm e}^{i\phi}/\sqrt{2} & 0 \\ B_{\rm q}\,{\rm e}^{-i\phi}/\sqrt{2} & 0 & B_{\rm q}\,{\rm e}^{i\phi}/\sqrt{2} \\ 0 & B_{\rm q}\,{\rm e}^{-i\phi}/\sqrt{2} & -B_z \end{pmatrix}. \quad (2)$$

The (spatially dependent) eigenvectors of Eq. (2) are

$$|\pm B\rangle = \left([B\pm B_z]\,{\rm e}^{i\phi}, \pm\sqrt{2}B_{\rm q}, [B\mp B_z]\,{\rm e}^{-i\phi}\right)^T/2B \quad (3)$$

and

$$|Z\rangle = \left(-B_{\rm q}\,{\rm e}^{i\phi},\ \sqrt{2}B_z, B_{\rm q}\,{\rm e}^{-i\phi}\right)^T/\sqrt{2}B \quad (4)$$

where $B = (B_{\rm q}^2+B_z^2)^{1/2}$. The $|+B\rangle$ and $|-B\rangle$ eigenvectors denote the strong- and weak- field-seeking states with eigenvalues $\pm B$, while $|Z\rangle$ is associated with the zero eigenvalue of $\mathbf{B}\cdot\mathbf{F}$. Through these eigenvectors we can see the fundamental technique behind the imprinting method of Ref. [23]; varying $B_{\rm q}$ (via b') and B_z over time, the condensate remains in a given eigenvector of $\mathbf{B}\cdot\mathbf{F}$, but transfers between the m_f states, accumulating angular momentum in the process. Some radial dynamics can occur as the B-field varies with time, but these dynamics separate out from the behaviour described by $\mathbf{B}\cdot\mathbf{F}$, and so are not addressed by our analytics. Later, when treating the Sagnac effect, the eigenvalues are modified slightly by the angular velocity term of Eq. (1). Again, it can be shown that the dominant spin dynamics decouple from the radial dynamics. This implication of spin-gauge symmetry is confirmed by the full 3D numerics.

To achieve the counterflow state (i.e., beam-splitting) we must initially prepare our condensate in the $|0\rangle$ spin-state with some dominating initial bias field in the z direction ($|B_z| \gg |B_{\rm q}(R_0)|$). This constitutes the $|Z\rangle$ state. The $|0\rangle$ initial state can be achieved through RF-pumping a $|-1\rangle$ (weak-field-seeking) condensate [36]. This can be carried out after transfer to an optical trap, where magnetic trapping is no longer required. Alternatively, a strong x (or y) bias field could be used to adiabatically transfer the atoms into a weak-field-seeking $|0\rangle$ (ZQ) state, then diabatically transferring these to the $|Z\rangle$ state by quickly switching off the x bias (this process can be somewhat destructive if the x bias is too large). With our initial condition now fixed in the $|Z\rangle$ eigenstate, the counterflow state is obtained by ramping $|B_z|$ down to zero over a period $T_{\rm s}$ [Fig. 1,] splitting the condensate into a superposition of spin up and spin down, as can be seen from Eq. (4). In our numerics, the quadrupolar field is characterised by an initial gradient $b' = 3.7$ G/cm, while the initial z bias field is set to $B_z = 50$ mG. We select the ramp-down period $T_{\rm s} = 22$ ms, selected to be one order of magnitude greater than the Larmor

precession time $T_L = 2\pi\hbar/(\mu_B g_F b' R_0) = 2.2$ ms, ensuring the spins follow the B-field adiabatically. As the atoms in a given spin state have an associated flow field, the condensate is now in a superpositional counterflow state. We note that, for $|B_z| \gg |B_q(R_0)|$, during a linear ramp-down of duration T_s the z bias would be dominant for most of the ramp-down, and so the effective transfer period would be too short. As such, we should carefully choose a smooth ramp-down with an exponentially decaying tail to avoid diabatic processes. We achieve this in our numerics using a suitably shifted and rescaled hyperbolic tangent function. Ramping too quickly can lead to radial excitations, which do not necessarily disrupt the splitting, but can prevent the spatial overlap of the counter-flowing components. During counterflow the system is still described by the $|Z\rangle$ eigenstate, and so if we now return B_z to its initial value (or any other value of suitably large magnitude) the entire condensate will return to $|0\rangle$, assuming no phase-shifting has occurred. We will use this method for recombination in our interferometry protocol.

With our beam-splitting and recombination protocols established, we can now consider the impact of a relative phase-shift, consistent with the approach described in Ref. [3]. Artificially imprinting a relative phase difference δ between the spin up and spin down components after the split (at some time when $B_z = 0$), we can re-write our counterflow state as a combination of all three eigenstates of $\mathbf{B}\cdot\mathbf{F}$. The weighting of these states is determined by δ:

$$|\Psi\rangle = \frac{1}{\sqrt{2}}\left(-\mathrm{e}^{i(\phi+\delta/2)}, 0, \mathrm{e}^{-i(\phi+\delta/2)}\right)^T \qquad (5)$$
$$= \sqrt{\frac{1+\cos(\delta)}{2}}|Z\rangle - i\sqrt{\frac{1-\cos(\delta)}{2}}\left(\frac{|+B\rangle + |-B\rangle}{\sqrt{2}}\right).$$

Ramping B_z back up implements the recombination, after which the $|\pm B\rangle$ eigenvectors are the $|\pm 1\rangle$ spin states, while the $|Z\rangle$ eigenvector is the $|0\rangle$ spin state. Hence, formally projecting our final state onto the zero spin state via the $|0\rangle\langle 0|$ projector (or, equivalently $|Z\rangle\langle Z|$) we obtain an interferometric signal based on the condensate fraction in the $|0\rangle$ state, i.e., $\int |\Psi_0(t_f)|^2 \mathrm{d}\mathbf{r} = [1+\cos(\delta)]/2$, where t_f is the time when our interferometry protocol ends. The populations of the different spin components can be observed by applying a field gradient in the z direction, resulting in Stern–Gerlach separation.

We now simulate prospective interferometry applications of this procedure, where Ω_z or B_z are nonzero during the interrogation counterflow period T_I. Assuming the counterflow state is well described by Eq. (5) (particularly that it is rotationally symmetric), we may combine the rotational and Zeeman terms of Eq. (1) by applying the $i\hbar(\mathbf{r}\times\mathbf{\Omega})\cdot\nabla$ operator to this state. The effect of the rotation is simply to offset the strength of the z bias field, which appears reduced (increased) as the coordinate system rotates with (against) the magnetic dipole precession. This gauge transformation can be expressed as $\tilde{B}_z \to \tilde{B}_z + \tilde{\Omega}_z$, where $\tilde{\mathbf{B}} = \mu_B g_F \mathbf{B}/\hbar\omega_\perp$ and $\tilde{\mathbf{\Omega}} = \mathbf{\Omega}/\omega_\perp$ are dimensionless quantities. Experimentally, $\tilde{B}_z \gg \tilde{B}_q \gg \tilde{\Omega}_z$ is typically achievable. Indeed, if $\tilde{\Omega}_z \gtrsim 0.2$ the system nucleates vortices, and as $\tilde{\Omega}_z \to 1.0$ the centrifugal force overcomes the optical trapping and the condensate's expansion is unconstrained [37, 38]. In this high $\tilde{\Omega}_z$ regime our transformation is no longer valid as the assumed rotational symmetry breaks when vortices enter the condensate. We will discuss the implications of this equivalency between $\tilde{B}_z$ and $\tilde{\Omega}_z$ later. Such a transformed system has analogous transformed eigenvectors. This means that, ramping down $|B_z| \to 0$,we are still in the $|Z\rangle$ eigenstate of $\mathbf{B}\cdot\mathbf{F}$, and therefore do not expect any phase difference between the $|\pm 1\rangle$ components to accumulate. In order to observe relative phase accumulation, we must have a superpositional counterflow state in the absence of a quadrupolar field. Carefully ramping down B_q with $B_z = 0$ achieves this aim and unpins the phases of the counterflowing components, but if there remains some small residual contribution $B_{zR} \neq 0$ then the system will (eventually) return to $|0\rangle$, as dictated by Eq. (4), and counterflow is lost. To avoid this restorative effect we must choose the ramp-down curve such that the B_q switch-off is diabatic in some sense. For example, this curve could be smoothly decaying at first and then cut off instantaneously before the point where $B_q \approx 10\times B_{zR}$, or fully continuous but ramped over a suitably fast timescale. In our numerics, the residual field was either zero or of the order of micro-Gauss, and so $T_s = 22$ ms was suitably fast to avoid recombination into $|0\rangle$. The key consideration should be reduction of the radial dynamics and heating associated with diabatic processes, noting that the smaller the residual field, the smaller the associated Zeeman energy, and so the less danger of heating. We also highlight that this restorative effect requires the residual field to satisfy $B_{zR} \ll B_q(R_0) \approx 1.57$ mG. This upper bound scales linearly with R_0 and b', and can easily be raised. In the complete absence of a magnetic field the hyperfine states become degenerate. In general this leads to undesirable spin-flips, which become more energetically allowable as $B \to 0$. We have previously noted that spin-flipping collisions are suppressed in the superpositional counterflow state. Another possible source of undesirable spin-flips is stray fields. However, assuming the field can be controlled

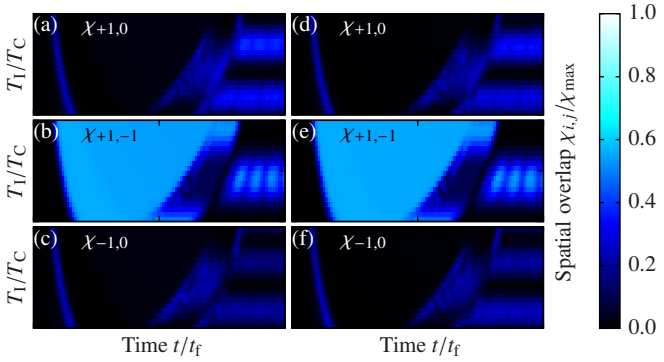

FIG. 2. (color online) Numerical simulation demonstrating overlap $\chi_{i,j}$ between the $|i\rangle$,$|j\rangle$ spin-states during counterflow interferometry. (a,b,c) show the overlap for Sagnac interferometry with varying interrogation times T_I giving varying accumulated phases δ_S. (d,e,f) show the Zeeman-energy interferometry case with phase difference δ_Z. All axes run over the range [0,1]. The overlap integral is scaled by the maximal value χ_{max}, achieved when the condensate is equally split and has the same spatial profile in both components.

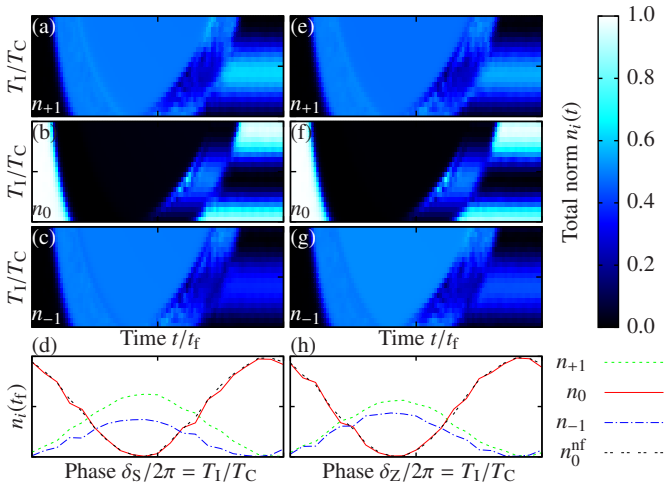

FIG. 3. (color online) Numerical simulation demonstrating the response of the system to different interrogation periods T_I, resulting in different accumulated Sagnac phases δ_S and Zeeman-energy phases δ_Z.(a-c,e-g) show how the norms of each spinor component vary with time. The x-axis is scaled by the total run time (t_f), which is increased to accumulate a larger phase difference $\delta_{S,Z}$. (d,h) show final interferometry curves at the final time t_f. All axes run over the range [0,1].

on the sub mG scale, such processes have a long associated timescale and can be ignored. Finally, we note that quantum and thermal fluctuations may be another source of undesirable spin-flips, but such analysis is beyond the scope of this Letter. A strategy to avoid undesirable spin-flips would be to purposefully retain a nonzero B_{zR}. Once the quadrupolar field is absent, the $|\pm 1\rangle$ components can evolve freely, and so accumulate a Sagnac phase δ_S for $\Omega_z \neq 0$, or a Zeeman-energy phase δ_Z for $B_{zR} \neq 0$. The magnitude of this phase can be quantified in terms of either the ring's enclosed area or the interrogation period T_I [3]. Allowing each component to perform the equivalent of one full circulation around the ring will cause the accumulation of a Sagnac phase $\delta_S = 2A\Omega_z m/\hbar$, as the ring will be doubly-enclosed by the counterflowing atoms. The particle velocity around the ring is given by the velocity-field of a vortex, $\mathbf{v} = (\hbar/m\rho)\hat{\phi}$, and so we determine the time for a single particle to fully circumnavigate the ring (such that $\rho = R_0$) to be $T_C = 2\pi R_0^2 m/\hbar = 2Am/\hbar = 156$ ms. The phase accumulated for an arbitrary interrogation time T_I is then $\delta_S = (T_I/T_C)2\Omega_z Am/\hbar = \Omega_z T_I$. The same arguments apply for the Zeeman-energy phase under the substitution $\Omega_z \rightarrow (\mu_B/\hbar)B_z$. After interrogation, restoring the quadrupolar B-field projects our phase-shifted wave-function onto the eigenstates of $\mathbf{B}\cdot\mathbf{F}$. Over the interrogation period the populations in the m_f (ZQ) states do not change. However, phases are accumulated with the effect that the populations in the $|\pm B\rangle$, $|Z\rangle$ basis are changed upon restoration of the quadrupolar field, and so the weighting of these eigenstates after interrogation differs from the initial weighting. This restoration and projection induces some radial oscillations as the $|\pm B\rangle$ eigenstates are respectively strong and weak-field-seeking. These oscillations can be seen in the overlap integrals shown in Figs. 1(c) and 2, however they do not affect the recombination as the radial dynamics decouple from the eigenvectors of $\mathbf{B}\cdot\mathbf{F}$. The recombination is achieved by ramping the z bias field back to a finite large value, thus re-encoding the phase information as populations in the different spin states [Eq. (5)].

Results of numerical simulations (using CUDA [39]) are displayed in Figs. 2 and 3. We performed full interferometry procedures for both rotational- and field-sensing scenarios, fixing $\tilde{\Omega}_z$ and $\tilde{B}_{zR}$ to be either 0.04 or zero respectively. Different phases accumulated over varying the interrogation times T_I. Fig. 2 displays the full time evolution of the density-density overlap integral $\chi_{i,j}(t) = \int |\Psi_i|^2|\Psi_j|^2 d\mathbf{r}$ for each interferometry run. In both cases, we observe good overlap during the counterflow phase for the adiabatic splitting procedure outlined above. When the quadrupolar field is restored, oscillations are evident as a result of the condensate now populating the $|\pm B\rangle$ eigenstates. After the recombination these oscillations are no longer present, confirming the robustness of the procedure implied by the separation of radial dynamics in the analytical treatment. The time evolution of the total norm $n_i = \int |\Psi_i|^2 d\mathbf{r}$ is displayed in Fig. 3. Population oscillations outlined by Eq. (5) are clearly evident at the end of the interferometry procedure. The interferometry cosine curves [Fig. 3(d,h)] are offset slightly as a result of minor phase accumulation during the quadrupolar ramp-down period. Furthermore, the curves deviate slightly from a true cosine due to the minor instability introduced by the g_s term. This was determined numerically by performing runs without this term, producing smoother curves. We note that the equivalency between $\tilde{\Omega}_z$ and $\tilde{B}_z$ require that care be taken in experimental measurements. The value of 0.04 used in the numerics corresponds simultaneously to $\Omega_z = 2\pi \times 6.4$ Hz and $B_z = 4.5\,\mu$G. As such, it should be relatively straightforward to make single-shot field measurements on the micro-Gauss scale, as large rotations should be absent. Similarly, it will be necessary to know the profile of a time-dependent angular velocity, so that a signal can be extracted from a time-series of measurements which may include exceedingly small background B-fields. Alternatively, an additional RF-pump could be applied half way through the interrogation phase, swapping the components into the opposite spin states and allowing any accumulated Zeeman phases to unwind during the remaining half of the interrogation.

To conclude, we have first outlined a new technique for generating long-lived superpositional counterflow states, a quantum-mechanical state of fundamental interest. We have then explored the application of this state to interferometry. Our setup maximises the classical Fisher information [20], and relies on adiabatic processes and so may be a candidate for large scale many-body quantum enhanced interferometry [18, 19]. Further investigations will explore the effect of quantum fluctuations and applications to ZASI.

The data presented in this Letter can be found in Ref. [40].

We thank A. L. Marchant, R. Bettles, C. Weiss, and S. Haine for useful discussions and the UK EPSRC (grant number EP/K03250X/1).

[1] A. Lenef, T. D. Hammond, E. T. Smith, M. S. Chapman, R. A. Rubenstein, and D. E. Pritchard, Phys. Rev. Lett. **78**, 760 (1997).
[2] T. L. Gustavson, P. Bouyer, and M. A. Kasevich, Phys. Rev. Lett. **78**, 2046 (1997).
[3] P. L. Halkyard, M. P. A. Jones, and S. A. Gardiner, Phys. Rev. A **81**, 061602 (2010).
[4] J. L. Helm, S. L. Cornish, and S. A. Gardiner, Phys. Rev. Lett. **114**, 134101 (2015).
[5] F. I. Moxley, J. P. Dowling, W. Dai, and T. Byrnes, Phys. Rev. A **93**, 053603 (2016).
[6] S. P. Nolan, J. Sabbatini, M. W. J. Bromley, M. J. Davis, and S. A. Haine, Phys. Rev. A **93**, 023616 (2016).
[7] M. J. Snadden, J. M. McGuirk, P. Bouyer, K. G. Haritos, and M. A. Kasevich, Phys. Rev. Lett. **81**, 971 (1998).
[8] A. Peters, K. Y. Chung, and S. Chu, Metrologia **38**, 25 (2001).
[9] J. M. McGuirk, G. T. Foster, J. B. Fixler, M. J. Snadden, and M. A. Kasevich, Phys. Rev. A **65**, 033608 (2002).
[10] S. Chu, A. Peters, and K. Y. Chung, Nature **400**, 849 (1999).
[11] H. Müller, S.-w. Chiow, S. Herrmann, S. Chu, and K.-Y. Chung, Phys. Rev. Lett. **100**, 031101 (2008).
[12] H. Müller, A. Peters, and S. Chu, Nature **463**, 926 (2010).
[13] P. A. Altin, M. T. Johnsson, V. Negnevitsky, G. R. Dennis, R. P. Anderson, J. E. Debs, S. S. Szigeti, K. S. Hardman, S. Bennetts, G. D. McDonald, L. D. Turner, J. D. Close, and N. P. Robins, New J. Phys. **15**, 023009 (2013).
[14] B. Canuel, F. Leduc, D. Holleville, A. Gauguet, J. Fils, A. Virdis, A. Clairon, N. Dimarcq, C. J. Bordé, A. Landragin, and P. Bouyer, Phys. Rev. Lett. **97**, 010402 (2006).
[15] G. M. Tino and F. Vetrano, Class. Quantum Grav. **24**, 2167 (2007).
[16] S. Dimopoulos, P. W. Graham, J. M. Hogan, M. A. Kasevich, and S. Rajendran, Phys. Rev. D **78**, 122002 (2008).
[17] P. W. Graham, J. M. Hogan, M. A. Kasevich, and S. Rajendran, (2016), arXiv:1606.01860.
[18] C. Gross, J. Phys. B **45**, 103001 (2012).
[19] A. J. Ferris and M. J. Davis, New J. Phys. **12**, 055024 (2010).
[20] S. A. Haine, Phys. Rev. Lett. **116**, 230404 (2016).
[21] T.-L. Ho, Phys. Rev. Lett. **81**, 742 (1998).
[22] T. Ohmi and K. Machida, J. Phys. Soc. Jpn **67**, 1822 (1998).
[23] T. Isoshima, M. Nakahara, T. Ohmi, and K. Machida, Phys. Rev. A **61**, 063610 (2000).
[24] S.-I. Ogawa, M. Möttönen, M. Nakahara, T. Ohmi, and H. Shimada, Phys. Rev. A **66**, 013617 (2002).
[25] Z. F. Xu, P. Zhang, R. Lü, and L. You, Phys. Rev. A **81**, 053619 (2010).
[26] J. Lovegrove, M. O. Borgh, and J. Ruostekoski, Phys. Rev. A **93**, 033633 (2016).
[27] D. M. Stamper-Kurn and M. Ueda, Rev. Mod. Phys. **85**, 1191 (2013).
[28] Y. Kawaguchi and M. Ueda, Phys. Rep. **520**, 253 (2012).
[29] K.-X. Sun, M. M. Fejer, E. Gustafson, and R. L. Byer, Phys. Rev. Lett. **76**, 3053 (1996).
[30] T. Eberle, S. Steinlechner, J. Bauchrowitz, V. Händchen, H. Vahlbruch, M. Mehmet, H. Müller-Ebhardt, and R. Schnabel, Phys. Rev. Lett. **104**, 251102 (2010).
[31] J. Mizuno, A. Rüdiger, R. Schilling, W. Winkler, and K. Danzmann, Opt. Commun. **138**, 383 (1997).
[32] M. Punturo *et al.*, Class. Quantum Grav. **27**, 084007 (2010).
[33] N. Mavalvala, D. E. McClelland, G. Mueller, D. H. Reitze, R. Schnabel, and B. Willke, Gen Relativ Gravit **43**, 569 (2010).
[34] A. Rakonjac, A. L. Marchant, T. P. Billam, J. L. Helm, M. M. H. Yu, S. A. Gardiner, and S. L. Cornish, Phys. Rev. A **93**, 013607 (2016).
[35] M. W. Ray, E. Ruokokoski, S. Kandel, M. Möttönen, and D. S. Hall, Nature **505**, 657 (2014).
[36] M.-S. Chang, C. D. Hamley, M. D. Barrett, J. A. Sauer, K. M. Fortier, W. Zhang, L. You, and M. S. Chapman, Phys. Rev. Lett. **92**, 140403 (2004).
[37] A. Aftalion and Q. Du, Phys. Rev. A **64**, 063603 (2001).
[38] P. Mason and A. Aftalion, Phys. Rev. A **84**, 033611 (2011).
[39] J. Nickolls, I. Buck, M. Garland, and K. Skadron, Queue **6**, 40 (2008).
[40] 10.15128/r1m900nt41q.